Complex Permeability And Magnetization Studies In Some Fe-Rich Soft Ferro-Magnetic Metallic Glasses

Prof. Debashis Das[1]

***Corresponding Author: -** Prof. Debashis Das
* [1]Assistant Professor, Department of Physics,Shibpur Dinobundhoo Institution(College), Howrah-711102,West Bengal, India,
Mail id-deba.debashis@gmail.com

Abstract-

To study the complex permeability spectra and magnetization using VSM for the following ferromagnetic metallic Glasses: (1) FINEMET ($Fe_{73.5}Nb_3Cu_1Si_{13.5}B_9$) ,(2) SAMPLE-1 ($Fe_{81}B_{12}Mo_7$) ,(3) SAMPLE-2($Fe_{80}B_{12}Mo_7Cu_1$), (4) SAMPLE-3 ($Fe_{82}B_{12}Mo_7Cu_1$),&(5) SAMPLE-4($Fe_{83}B_{12}Mo_5$) .

Keywords - Amorphous Material, metallic glasses, permeability, Complex permeability. Magnetization.

DOI Number: 10.14704/nq.2022.20.9.NQ44361 Neuro Quantology 2022; 20(9):3119-3128

1.1 Introduction

Melt-spun ribbons of metastable, soft ferromagnetic alloys recently gained renewed interest as good candidate for active elements of magneto-elastic sensors. In these applications, the magneto-elastic response is generally enhanced in materials where either a nearly complete structure relaxation or a partial nanocrystalization is induced. The Complex permeability spectroscopy has been useful for studying magnetization processes in ferromagnetic material because the static permeabilities and relaxation frequencies for the reversible and irreversible magnetization processes could be determined from the spectra. The permeability in metallic glass samples show two dispersions associated with irreversible domain wall motion and reversible magnetization. These magnetization processes are known to be influenced by external and internal stress around the defects.

In this paper we have studied the complex permeability spectra for the following ferromagnetic amorphous alloys: (1) FINEMET ($Fe_{73.5}Nb_3Cu_1Si_{13.5}B_9$), (2) SAMPLE-1 ($Fe_{81}B_{12}Mo_7$), (3) SAMPLE-2($Fe_{80}B_{12}Mo_7Cu_1$), (4) SAMPLE-3 ($Fe_{82}B_{12}Mo_7Cu_1$),&(5) SAMPLE-4($Fe_{83}B_{12}Mo_5$) at zero external field.

1.2 Method of Study for measurement of complex permeability

The real and imaginary part of the complex permeability, $\mu(f) = \mu'(f) - j\,\mu''(f)$, were measured using Agilent 4294A precision Impedance analyzer in the frequency range of 1-20 MHz at room temperature T=300K. The setup and procedure for the experiment was same as that described in chapter 3. The amplitude of the AC current applied to the small solenoid coil around the rectangular sample was kept to a constant value during the frequency sweep for the measurement of the permeability spectra. The length of the coil was intentionally made shorter than the length of the sample to reduce the demagnetization effect.

The real and imaginary parts of the complex permeability were determined as follows:

$\mu'(f) = \{L(f)-L_0(f)\}/ L_0(f)$,

$\mu''(f) = \{R(f)-R_0(f)\}/ R_0(f)$,where L and R are the equivalent inductance and resistance of the solenoid with sample, respectively, while L_0 and R_0 refer to those of empty solenoid.

Theory

The permeability of the ferromagnetic sample placed inside a coil of uniform turns is dependent on the measured inductance of the coil. The complex permeability is given by $\mu(f) = \mu'(f) - j\,\mu''(f)$. The real and the imaginary part of the permeability is given as :

$\mu'(f) = \{L(f)-L_0(f)\}/ L_0(f)$,

$\mu''(f) = \{R(f)-R_0(f)\}/ L_0(f)$,
where L and R are the equivalent inductance and resistance of the solenoid with sample, respectively, while L_0 and R_0 refer to those of empty coil.
Thus we can write the relative permeability as :

$$\frac{\mu}{\mu_0} \alpha \frac{L}{L_0}$$

Now, the magnetic susceptibility is related to the permeability as, $\mu_r = \chi + 1$.
Thus, a measure of the susceptibility gives the variation of the permeability and hence the inductance. In the following experiment we have measured the variation of susceptibility with temperature.

1.3 Method of Study for measurement of magnetization by using VSM.

Vibration Sample Magnetometer (VSM)

The VSM is the basic instrument for characterization of magnetic materials. Science, its invention some forty years ago, it has become the workhorse in both laboratory and production environments for measuring the basic magnetic properties of materials as a function of magnetic field and temperature.
A vibrating sample magnetometer (VSM) operates on Faraday's Law of Induction, which tells us that a changing magnetic field will produce an electric field. This electric field can be measured and can tell us information about the changing magnetic field. A VSM is used to measure the magnetic behavior of magnetic materials.
The Vibrating Sample Magnetometer (VSM) is based on vibrating a sample in a magnetic field to produce an alternating emf within a set of suitably placed pick-up or sensing coils. This induced emf is directly proportional to the magnetic moment m or magnetization M of the sample under test. VSM's are used widely since magnetic properties can be measured for a diverse range of sample sizes and configurations, i.e., powders, solids, single crystals, thin films, and liquids, and because they are particularly well suited to allow measurements at both low and high temperatures.
The VSM instrument is schematically shown in Fig6.1, employs an electromagnet, which provides the magnetic field (DC), a vibrator mechanism to vibrate the sample in the magnetic field, a detection coil, which generate the signal voltage due to changing flux emanating from the vibrating sample. The output measurement displays the magnetization M as a function of field H. The VSM represents by far the most commonly used type of magnetometer. In the following sections, we discuss the main components of the VSM, the capabilities and limitations on the generation and control of magnetic field, the signal and noise consideration in optimizing sensitivity, and precautions that must be exercised in order to get the best performance.

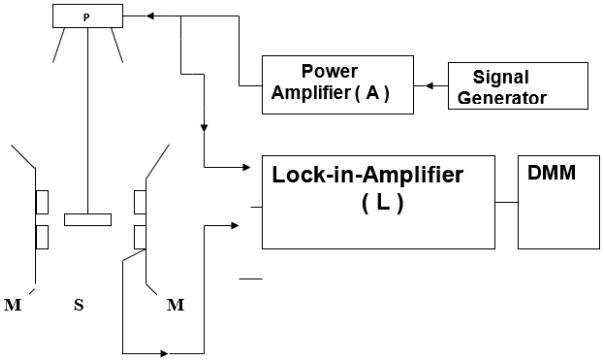

Figure **:** The schematic of VSM setup with different Components.

M → Magnet Poles
P → Audio Speaker
S → Sample
DMM → Digital Multimeter

1.3.2 Operational Principle

The VSM is based on a simple principle. A small sample of a given geometry is magnetized and allowed to vibrate in proximity of coils. An e.m.f. is induced is the coils as the flux linked with the coils changes due to the vibration of the sample. This induced e.m.f. is proportional to the Magnetic Moment of the sample. The proportionality constant depends on a number of factors like the shape of the sample, coil geometry, number of turns of the coil etc. Foner realized an experimental setup on this principle.
The sample S placed at the bottom of a stainless steel rod is attached to the center of a speaker. The speaker is excited by low frequency (82 Hz) e.m. wave from a power amplifier A which in turn is activated by signal from a frequency generator G. The sample is placed at a region of homogenous magnetic field of electromagnet M. Two pairs of coils are fixed to opposite faces of

electromagnet. Each coil has 200 turns and are having nearly same self-inductance. The coils C at each face of pole piece are connected in series opposition so that the induced signal gets doubled when sample vibrates about its mean position. Finally the coils at two faces are so connected that the signals are added up. The signal is measured by a phase sensitive detector (Lock-in-Amplifier L). The reference signal to the lock –in –Amplifier is obtained from the signal generator. The static magnetic field is generated by electromagnet, which is powered by D.C. power source.

1.3.3 Magnetization Measurement: VSM Sensitivity

The voltage V measured across the sensing coils in a VSM can be expressed as the product of four contributing sources:

$$V = MAFS$$

Where M = magnetic moment of the sample, A = amplitude of vibration, F = frequency of vibration, S = sensitivity function of the sensing coils.

The considerations, which determine the optimal setting of each of these components, are as follows:

(a) Magnetic moment of the sample M

This is the product of the magnetization of the sample (magnetic moment per unit volume) times the volume of the sample. There is not much we can do about the sample magnetization, since it is an intrinsic property of each material, but the selection of the sample volume can, in most cases, provide a great deal of latitude for optimal choice. In general, one prefers to use larger samples in order to get a larger signal and a better SNR. The precautions that must be exercised relate to the impact this may have on field uniformity, maximum required field, sensing coil configuration, dynamic range of the signal processor, vibrator load tolerance, and compatibility with optional systems such as cryostats and ovens. Clearly, a larger electromagnet provides better choices for optimal selection of sample sizes.

(b) Amplitude of vibration A

A large vibration amplitude increases system sensitivity, provided that the sensing coils are big enough to capture the large sample excursions with uniform sensitivity. Care should also be taken to avoid harmonic distortions.

(c) Frequency of vibration F

Whereas a higher vibration frequency leads to higher sensitivity, there are some basic constraints that limit the maximum usable frequency:

Objectionable audio emanating from the vibrator.

Eddy currents generated in conducting samples and/or substrates.

The vibration frequency chosen must be away from any harmonics or sub harmonics of power frequencies to minimize noise.

(d) Sensing coil sensitivity S

In general, the sensitivity increases by increasing the coupling between the flux emanating from the sample and the sensing coils. The coupling of the sample flux to the sensing coils is a strong inverse function of the distance between the sample and the coils. However, a small distance implies more critical sample mounting and larger errors resulting from any differences between the shape of the sample and that of the calibration standard. Increasing the number of turns in the sensing coils increases the signal, but for a fixed coil volume, also increases the resistance of the coils, which results in larger Johnson noise. Therefore, more turns improves the sensitivity only if Johnson noise of the coils is not the limiting noise factor in the system. Also, increasing the number of turns in the sensing coils tends to make balancing and impedance matching more difficult.

Noise and SNR

The sensitivity of the VSM generally depends on only two factors:

Background signals

The Signal-to-Noise ratio (SNR)

The distinction between background signals and noise is that the former includes disturbances which are not random in time (are either constant or vary, as a function of some parameter such as the applied field, the applied field direction, the vibration amplitude, etc.) whereas the latter includes disturbances which are random. Background Signals:

The main sources of background signals are:

1. The sample holder signal, the sample substrate signal, or any combination of

these. The usual procedure to correct for these disturbances is to make a measurement without the sample and subtract the results from the measurement made with the sample. To the extent that the measurements are reproducible, these background signals can be canceled out.

2. Vibration of the sense coils caused by mechanical coupling from the vibrator or acoustic coupling from the sample holder. Remedies for these include a high level of vibrational isolation of the sense coils, and extreme care taken in the balancing of the coils and the stability of the magnetic field at the time of each sampling of the magnetic moment. Other proprietary techniques are used to further reduce the transmittance of vibrations to the senses.
3. Signals induced by the motion of the vibrator through induction in wire loops or from the drive wires to the vibrator. These should be field independent and are observable even without a sample holder. A solution can usually be found by better shielding.
4. Signals from other power sources and machinery (both electrical and vibrational). The solution is to keep far away from these sources and their frequencies.

Noise in VSM systems

In most instances, noise presents the most limiting constraint in improving the sensitivity of VSM systems. To the extent that the noise sources are random, they can be reduced significantly by filtering or averaging at the expense of extending the measurement time. Therefore, when stating VSM sensitivities or noise levels, it is essential to also state the time constant of the measurement. In addition to the "random" noise, which has a constant average strength, one may encounter modulation noise due to the fluctuations of the signal itself and enter it as a fixed percentage of the signal. Since modulation noise is not really random, filtering or averaging is ineffective. The main sources of noise include the following:

• Electronic noise

Examples of this include Johnson, Shot, and 1/f noise, with only
Johnson noise being significant in typical VSM systems.
The Johnson noise is given by:

$$V_{noise,\ RMS} = (4kTR.f)^{1/2}$$

where:
k is Boltmann's constant
T is the temperature in degrees K
R is the resistance of the coils in Ohms
.f is the bandwidth of the measurement in Hz. This is usually the limiting noise
source in VSM systems.

• Electrical noise

There are various sources of this type of noise:

- Induction in wire loops due to power sources, computers, etc. To minimize the problem, signal cables should be twisted, shielded and symmetrical.
- Ground loops should be avoided.
- Amplifier noise arising from the involved electronics and quantization of the A/D converter.

• Modulation Noise

Examples of variations are the amplitude or the frequency of the vibrator due to thermal drift. A well-designed feedback system and a temperature-independent or temperature-controlled reference source are used to keep this disturbance at a low level.

1.3.4 Technique involved in the measurements by VSM

The samples that we had investigated were all in the form of ribbons. Now to place the samples in the VSM set up we cut the samples into small pieces with the dimensions of 2 cm in length, and 3 mm in breadth. Now we took four of such pieces of the sample and pasted them to each other. This made such thin samples quite thick and strong. Now we covered the attached pieces of the sample by a film of Teflon and celotape for added binding. After having prepared the sample fit to be placed in our VSM setup, we attached the sample in the groove provided at the end of the steel rod of the VSM as shown in the figure. All ingredients used for converting the samples originally in ribbon shape to that suitable to be placed in the VSM were nonmagnetic in nature. This ensured that no stray or added signals were added up with the original signal coming from the sample itself. After the sample was placed in the VSM, measurements were taken by varying the current in the power source, which in turn varied the magnetic field (H). The magnetic field

was generally varied between +6000 Gauss to –6000 Gauss. The positive and negative magnetic field was obtained by reversing the direction of the current in the loops.

Saturation Magnetization

In this particular study we have performed systematic measurement for the study of the Magnetization curves from which we have obtained the values of saturation magnetization of the sample under various concentration of Fe in the presence of other materials.

For each of the samples the Magnetization obtained was in μVolts. So each time the magnetization was converted to its usual unit i.e. in emu per gram by standardizing with the standard value of Saturation Magnetization of Nickel (~54 emu/gm). Then the Magnetization (emu/gm) versus the applied magnetic field (Gauss) was plotted. The M_S values are calculated by fitting the curve near saturation region, using

$M=M_0 - a/H + b/H^2$ (approach to saturation)

The spontaneous magnetization (M_{sp}) for the samples was obtained from arrott plot, in the high field region, by extrapolating H/M (gauss-gm/emu) versus M^2(emu/gm)^2 .

1.4.1 Techniques of Preparation

A number of techniques which provide cooling rates from 1 K/sec to 10^{15} K/sec have been used to produce glassy materials. The normal quenching methods used in the metallurgical industries have quenching rates of 1 to 10^3 k/sec. These are however insufficient for producing glassy or amorphous metals or metalloids and metal-metal alloys which require cooling rates of 10^6 K/sec. For this purpose several rapid liquid quenching techniques have been developed.

Melt Spinning

Among the most commonly used rapid liquid quenching techniques today is the melt spinning. This technique has the advantage of giving long ribbons having uniform cross-section and reproducible properties. This is the reason for its being used for large scale commercial production of amorphous alloys.

A melt spinner consists of a disc, usually of copper, which is rotated at a high speed to generate a rim velocity of more than 50 $msec^{-1}$. A properly superheated molten alloy is ejected under high pressure through a fine nozzle at the bottom of a refractory tube on to the spinning disc. The alloy is melted by rf induction heating under an inert helium or argon atmosphere.

Sputtering

Besides rapid liquid quenching by melt spinning, the most widely used technique for the formation of glassy metals is sputtering. Sputtering is defined as the process by which atoms or molecular groups are released from a target (cathode) under the bombardment of positive ions.

Ion Implantation

Recently a technique called “ion implantation” has been extensively used for modifying the properties of the surface layers of thin films specially of semiconductors. In this technique high speed ions are allowed to impinge on the surface. These ions travel a short distance and get embedded within the top few atomic layers (10 nm to 1 μ m) of the material. In this process the quenching rate is estimated to be about 10^{14} K/sec. It is possible to produce amorphous Para-surface layers in crystalline solids by implanting ions in high dose.

1.4.2 Preparation of Polycrystalline Sample

These samples were prepared by induction melting of required amount of “spec-pure” grade constituent elements. Initially the pure elements are cleaned with organic solvent HNO_3, after which the required amounts are cut and weighed carefully. A water cooled induction furnace with a maximum power of 7 kW, fed by an “Ajax Magnothermic Converter” (which converts the line-frequency of 50 Hz to a value between 20 to 40 kHz depending on power consumption), is used for melting. The required elements are kept in a high quality alumina crucible which is then placed in a graphite susceptor. Now the whole thing is put in a vacuum sealed quartz tube inside the furnace. The quartz tube is repeatedly evacuated to 10^{-3} Torr and flushed with high purity argon gas. Finally, it is sealed after filling the argon gas at much less than atmospheric pressure. During the heating process, an optical pyrometer is used to monitor the increase in

temperature. As soon as the elements get melted, the furnace is turned off to cool the melt in the furnace.

All the homogenized alloys in the bulk form are the cold rolled (30% cold work) in the form of a sheet and cut into thin rectangular strips as well as in needle forms for various transport and magnetic measurements. All the pieces are then finally annealed in argon atmosphere in a sealed quartz tube for 30 hours at 1050 ^{0}C to reduce strain in the specimen introduced due to cold work. These annealed samples are then quenched fast to room temperature to brine

1.5 Results for complex permeability Study

1.5.1 Sample 0 : FINEMET ($Fe_{73.5}Nb_3Cu_1Si_{13.5}B_9$)

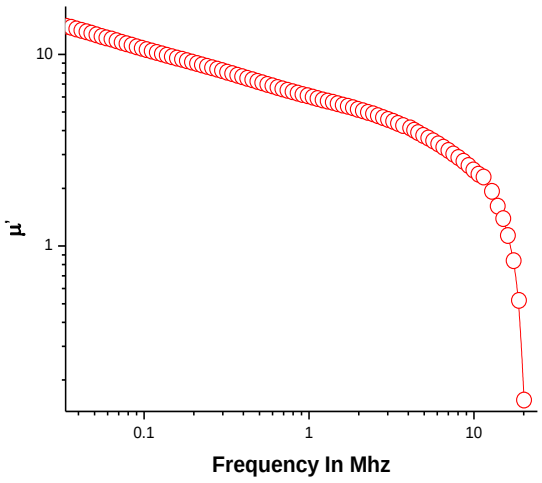

Figure 1.5.1(a) Real part of the permeability spectra at 20mAmp ac field

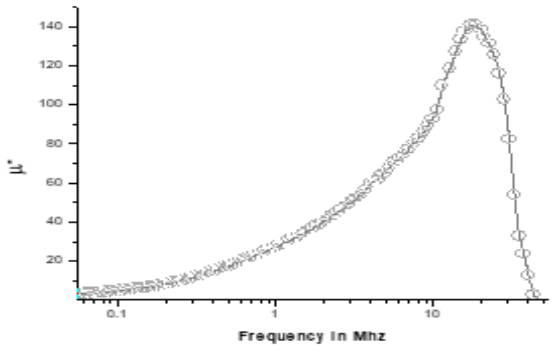

Figure 1.5.1(b) Imaginary part of the permeability spectra at 20mAmp ac field

1.5.2 Sample 1 : ($Fe_{81}B_{12}Mo_7$)

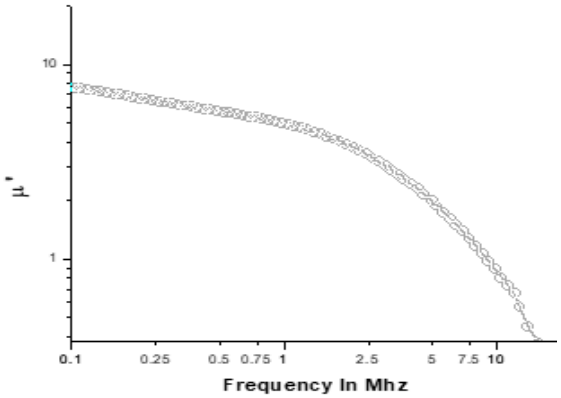

Figure 1.5.2(a) Real part of the permeability spectra at 20mAmp ac field

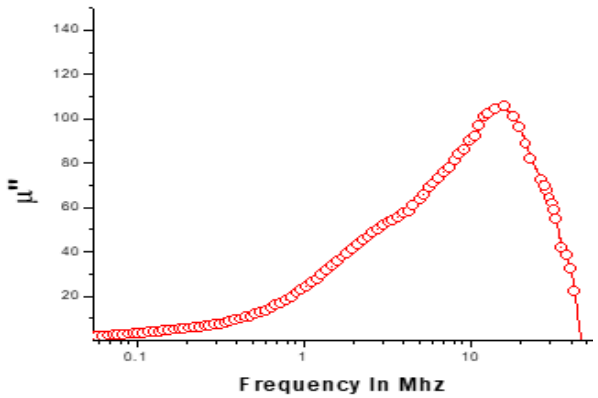

Figure 1.5.2(b) Imaginary part of the permeability spectra at 20mAmp ac field

1.5.3 Sample2 : ($Fe_{80}B_{12}Mo_7Cu_1$)

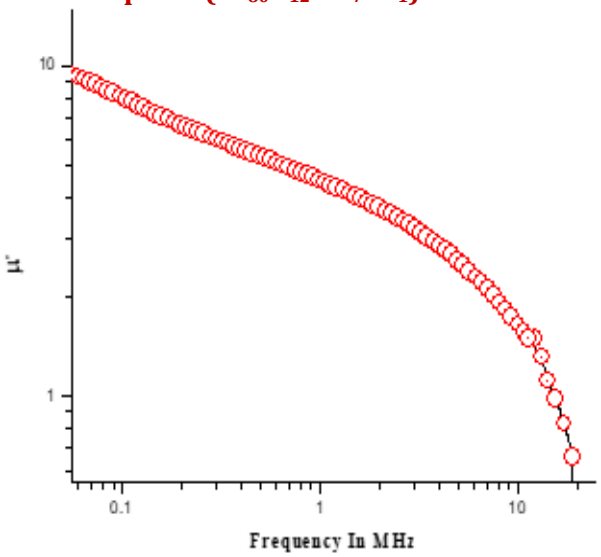

Figure 1.5.3(a) Real part of the permeability spectra at 20mAmp ac field

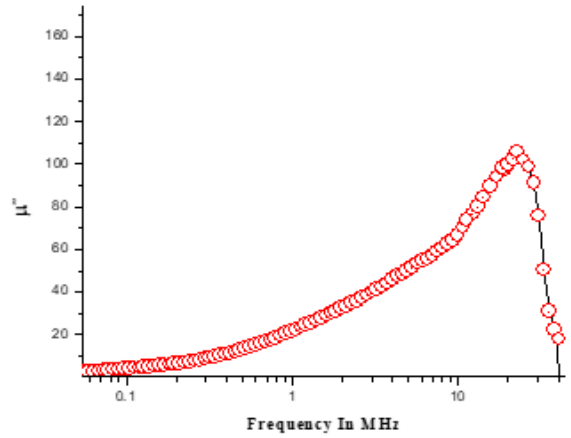

Figure1.5.3(b) Imaginary part of the permeability spectra at 20mAmp ac field

1.5.4 Sample 3 : ($Fe_{82}B_{12}Mo_7Cu_1$)

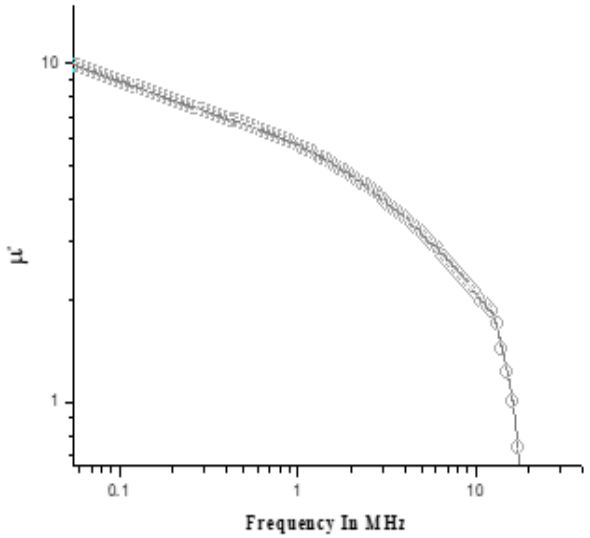

Figure 1.5.4(a) Real part of the permeability spectra at 20mAmp ac field

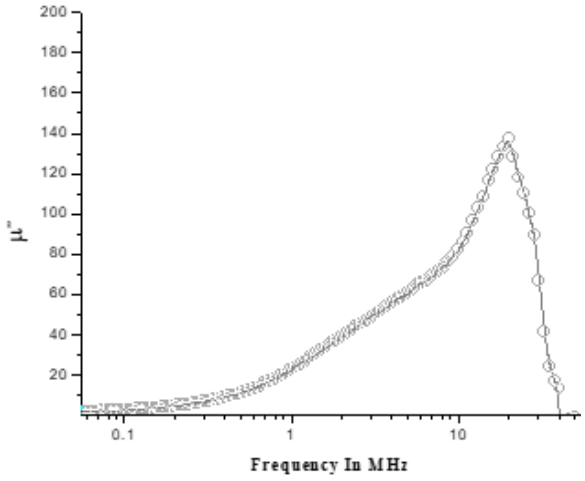

Figure 1.5.4(b) Imaginary part of the permeability spectra at 20mAmp ac field

1.5.5 Sample 4 : ($Fe_{83}B_{12}Mo_5$)

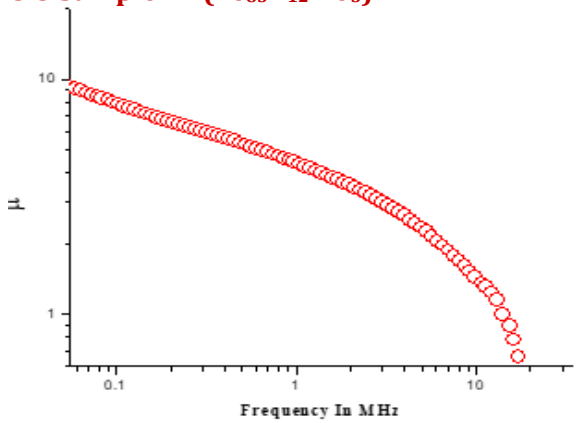

Figure 1.5.5(a) Real part of the permeability spectra at 20mAmp ac field

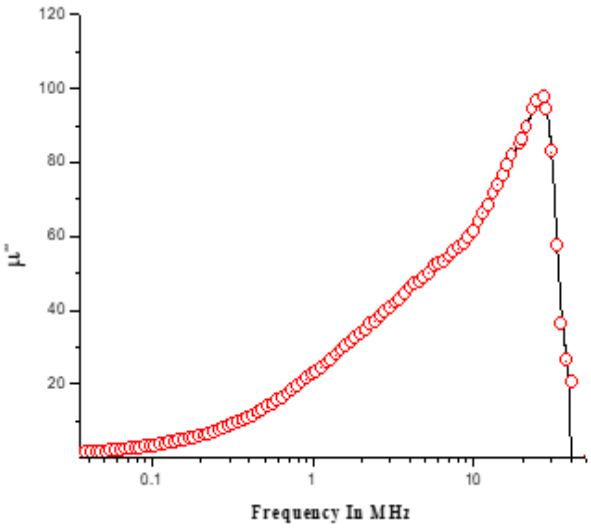

Figure 1.5.5(b) Imaginary part of the permeability spectra at 20mAmp ac field

1.6 Discussions

From the study of the permeability spectrum it is seen that the real part of the permeability remains constant for low frequencies but reduces as we go to higher frequency region. While the variation of the imaginary part with frequency was found to increase at first then decrease. The imaginary parts of permeability show a typical Debye type relaxation. Also in the higher frequency range, the variation of permeability values was observed to be independent of the applied ac magnetic field, provided by the ac current passing through the coil. The Relaxation frequency f_o for different samples were measured from the maximum in the imaginary part of complex permeability.

The analysis of the complex permeability is rather critical and can be done by taking the

variation of the permeability at small applied ac field, of the order of mOe. The complex permeability can be described by the sum of two decomposed relaxation as follows:

$$\mu^*(f) = \mu'(f) - j\mu''(f)$$
$$= \mu'_{lo}(f) + \mu'_{hi}(f) - j\{\mu''_{lo}(f) + \mu''_{hi}(f)\}$$
$$= 1 + \frac{\mu_{lo}(h_0)}{1+(f/f^0_{lo})^2} + \frac{\mu_{hi}(h_0)}{1+(f/f^0_{hi})^2} - j\left(\frac{\mu_{lo}(h_0)(f/f^0_{lo})}{1+(f/f^0_{lo})^2} + \frac{\mu_{hi}(h_0)(f/f^0_{hi})}{1+(f/f^0_{hi})^2}\right)$$

where μ_{lo} and f^0_{lo} are the permeability magnitude and the relaxation frequency in the low-frequency region; μ_{hi} and f^0_{hi} are those in the high frequency region. Here h_0 is calculated from the solenoid geometry.

The figure 1.5 shows the temperature variation of inductance of the FINEMET ($Fe_{73.5}Nb_3Cu_1Si_{13.5}B_9$), Sample-1 ($Fe_{82}B_{12}Mo_7Cu_1$) and Sample-2 ($Fe_{83}B_{12}Mo_5$) amorphous ribbon after normalizing by its room temperature value. The sharp drop in their inductance indicates the transformation of the material from ferromagnetic to paramagnetic state. The Curie temperature (T_c = 568.53K, 365.1K and 385K) was estimated from the derivative of the inductance plot. Just before the transition temperature (T_c) Hopkinson peak was observed. The appearance of the Hopkinson peak in this soft ferromagnetic amorphous material at low applied ac driving field is mainly due to domain wall motion and hysteretic effect.

2. Results for magnetization Study (Experimental Results)

2.1 Plot for FINEMET ($Fe_{73.5}Nb_3Cu_1Si_{13.5}B_9$)

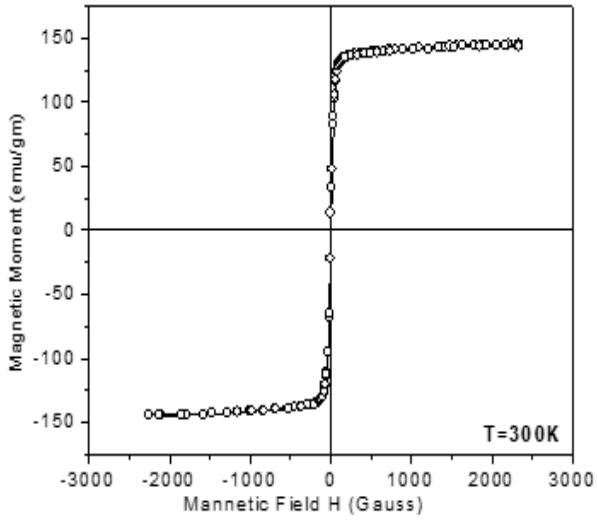

Figure(0): M Vs H Plot for FINEMET($Fe_{73.5}Nb_3Cu_1Si_{13.5}B_9$)

2.2 Plot for SAMPLE-1 ($Fe_{81}B_{12}Mo_7$)

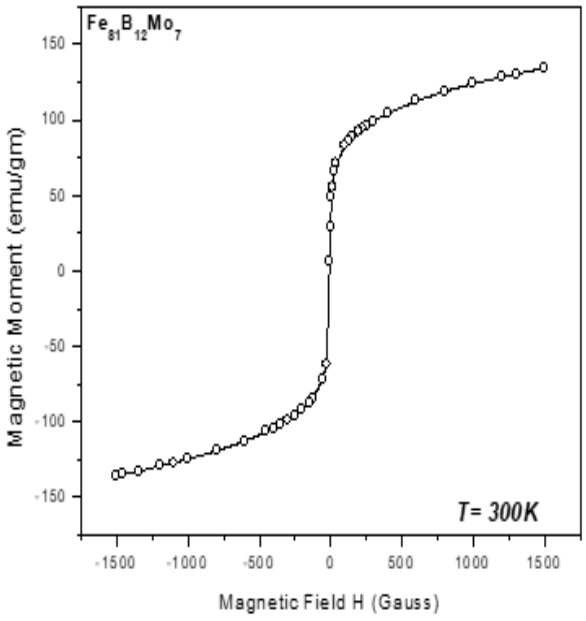

2.3 Plot forSAMPLE-2 ($Fe_{80}B_{12}Mo_7Cu_1$)

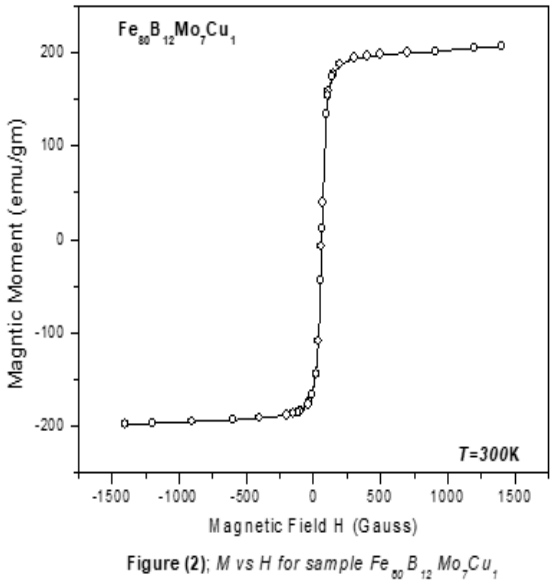

Figure (2); *M vs H for sample* $Fe_{80}B_{12}Mo_7Cu_1$

2.4 Plot for SAMPLE-3 ($Fe_{82}B_{12}Mo_5Cu_1$)

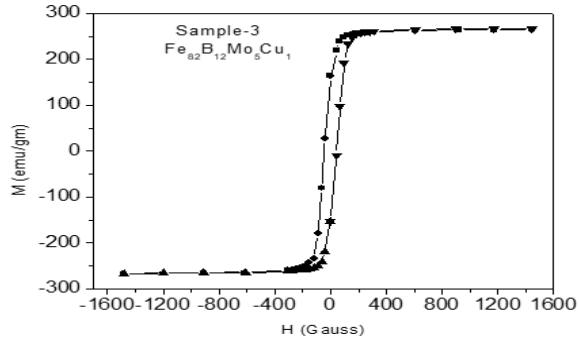

Figure(3); M vs H sample Fe_{82} B_{12} Mo_5 Cu_1

2.5 Plots for SAMPLE-4 ($Fe_{83}B_{12}Mo_5$)

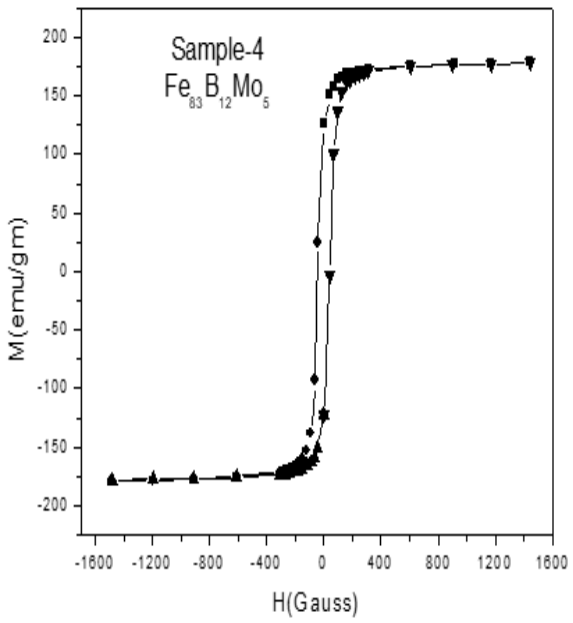

Figure(4); M vs H sample $Fe_{83}B_{12}Mo_5$

2.6 Comparative plot

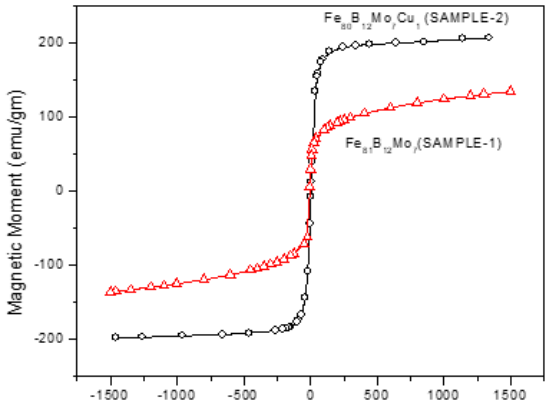

Figure (5); *Comparative Plot of M vs H for $Fe_{80}B_{12}Mo_7Cu_1$ (S2) and $Fe_{81}B_{12}Mo_7$(S1)*

2.7 Discussion

In this section we have systematically studied the magnetic properties, mainly the magnetic moment versus applied magnetic field (M vs H) curve, as well as the saturation magnetization of the alloys with variations in the atomic concentrations of magnetic material present in it. The amorphous materials under consideration are FINEMET ($Fe_{73.5}Nb_3Cu_1Si_{13.5}B_9$), SAMPLE-1 ($Fe_{81}B_{12}Mo_7$), SAMPLE-2 ($Fe_{80}B_{12}Mo_7Cu_1$), SAMPLE-3 ($Fe_{82}B_{12}Mo_7Cu_1$), and SAMPLE-4 ($Fe_{83}B_{12}Mo_5$). The saturation magnetization was found to depend on number of parameters.

3. Conclusions

From the analysis of the permeability spectra it can be seen that the real part of the permeability, for high frequency (~20 MHz), remains almost constant. This signifies that these materials could be used in device applications. A small or large fluctuation in the frequency does not change the property, i.e. permeability, of the sample. If μ changes by a considerable amount then the material will no longer act as ferromagnetic material, hence changing the property.

The complex permeability spectrum was studied for the samples. The real and the imaginary part of the permeability were plotted as a function of frequency. If we take the real value of permeability, it decreases very slowly (i.e. remain almost constant) upto ~10 MHz. In case of imaginary part of complex permeability it increases with frequency up to ~ 10 MHz. At about 20 MHz both the values of complex permeability go to the zero value. So in ac application we cannot use this material beyond this frequency limit.

From the above study of the magnetization it can be concluded that the samples under consideration are highly soft ferromagnetic materials, as the coercivity is very low. Spontaneous magnetization is the term used to describe the appearance of an ordered spin state (magnetization) at zero applied magnetic field in a ferromagnetic or ferrimagnetic material below a critical point called the Curie temperature or T_C. At temperatures above T_C, the material is paramagnetic and its magnetic behavior is dominated by spin waves or magnons. In the project we have systematically studied the magnetic properties, mainly the magnetic moment versus applied magnetic field (M vs H) curve, which is related in spontaneous magnetization. From the above figure SAMPLE-3 and SAMPLE-4 shows narrow hysteresis whereas SAMPLE-0, SAMPLE-1 and SAMPLE-2 shows no hysteresis.

Soft ferromagnetic materials has narrow hysteresis loop hence they could be magnetized or demagnetized easily. Thus they could be used in magnetic read / write heads. These materials are generally associated with electrical circuits where they are used to amplify the flux generated by the electric currents. These

materials can be used in a.c. as well as d.c. electrical circuits.

We have systematically studied the magnetic properties, mainly the change of magnetic moment with the applied magnetic field. We observed that the alloys are strongly ferromagnetic and are magnetically soft. We can thus conclude that, if we introduce some amount of Mo for the sample $Fe_{82}B_{12}Mo_5Cu_1$ in place of Fe ion we get decreased value of magnetic moment. Now if we increase the Cu content for the same sample again we get increased magnetic moment.

The materials under study have very less coercivity and remnant magnetization. So, these materials can be used as soft ferromagnetic device applications, like magnetic read/write head. These materials are generally associated with electrical circuits where they are used to amplify the flux generated by the electric currents.

References

A Sarkar, AK Das; Giant junction magnetoresistance effect in ferromagnet/semiconductor heterostructures; Journal of Applied Physics,2013.

A Ahmad , AK Das; Size-dependent Structural and magnetic properties of disordered Co2FeAl Heusler alloy nanoparticles; Journal of Magnetism and Magnetic Materials,2019

S Mandal , J Panda, TK Nath ; Investigation of the critical behaviour and magnetocaloric effect in Y-Fe49Ni29Cr22 disordered austenitic stainless steel alloy by using the field dependence of magnetic entropy change; Journal of Alloys and compounds,2015.

SK Mandal, TK Nath; Temperature dependence of solubility limits of transition metals (Co, Mn, Fe and Ni) in ZnO nanoparticles; Applied physics letters,2006.

S Chattopadhyay, TK Nath ; Enhancement of room temperature ferromagnetism of Fe-doped ZnO emitaxial thin films with Al co-doping; Journal of Magnetism and magnetic Meterials,2011.

Investigation of room temperature multiferroic properties in sol-gel derived gadolinium, cobalt doped BiFeO3 nanoceramics *by* Das S., Sahoo R. C., Nath T. K. **Journal of Applied Physics** 127 054101.1-054101.10 (2020).

Large ferromagnetism and dielectric behaviour in chemically synthesized 10% Co doped BiFeO3 multiferroic nanoceramics *by* Nath T. K., Das S. , Sahoo . C. **Materials Today** 11 719-723. (2019).

Acknowledgement:

I want to acknowledge my project guide Dr. Tapan Kumar Nath (Professor IIT- Kharagpur) for introducing me in Condensed matter physics. Also I thankful to Dr. Sourav Marik for helping the experiments in the IIT-Kharagpur Lab.